Hindawi
Mathematical Problems in Engineering
Volume 2020, Article ID 5960973, 9 pages
https://doi.org/10.1155/2020/5960973

Research Article

Influence of the Curvature of the Multipoint Die for Flexible Multipoint Stretch Bending on the Quality of Aluminum Profile

Yi Li[1], **Rui Li**[1], **Ce Liang**[1], **Jicai Liang**[1,2] and **Fei Teng**[3]

[1]*Key Laboratory of Automobile Materials, Ministry of Education, and College of Materials Science and Engineering, Jilin University, Changchun 130025, Jilin, China*
[2]*Roll Forging Research Institute, Jilin University, Changchun 130025, Jilin, China*
[3]*School of Mechanical and Vehicular Engineering, Changchun University, Changchun 130000, Jilin, China*

Correspondence should be addressed to Ce Liang; liangce@jlu.edu.cn

Received 1 September 2019; Revised 24 November 2019; Accepted 11 December 2019; Published 31 January 2020

Academic Editor: Mohamed Shaat

The finite element numerical simulation method was used to study the stretch-bending process of asymmetric L-section aluminum alloy profiles. The geometrical parameters of the multipoint dies (MPDs) are studied to influence the shape accuracy and springback of the L-section profile after bending. The results show that the profile curvature of the MPD after the profile is bent has a great influence on the stress-strain distribution, springback value, and shape accuracy. In order to obtain uniform stress-strain of the profile and reduce the springback and shape error, the MPD is optimized by numerical simulation analysis, which has a certain reference value of providing a theoretical basis for the rational design of the flexible stretch-bending.

1. Introduction

Lightweight is an important issue for the current automotive industry and rail transit system. Automotive lightweighting can be achieved by optimizing the body frame design and using lightweight materials. Aluminum profiles have been widely used in automotive and rail transit support structures due to their low density, high strength, and easy recycling [1]. Stretch-bending is a combining forming process of stretching and bending. And the tangential tension is applied during the bending process at the same time. The stretch-bending method adopted in this paper is based on P-M-P method of the arm pull bending machine, that is, the prestretching, followed by the stretch-bending forming, and finally the poststretching; the method can effectively reduce the springback and residual stress [2].

With the improvement of people's living standards, low cost and small batch production of various components will become the main way of industrial manufacturing in the future [3, 4]. Flexible multipoint stretch-bending technology is a flexible and rapid manufacturing technology, which can use the way of the MPD adjustment method that is used to change the curvature of the MPD in order to compensate springback after unload [5]. And the target shape of the profile in the same section is not much different, a set of MPDs can be shared to reduce the production cost.

It is difficult for complex cross-sectional profiles to bend in the horizontal direction without unloading condition to meet accuracy requirements through the traditional solid die [6, 7]. For the flexible multipoint stretch bending, in addition to the influence of the process parameters on the bending and forming effect, the solid die composed of a plurality of MPD bodies also has a great influence on the forming effect. Lin et al. determined the suitable number of MPDs for complex cross section profiles in stretch bending to reduce springback [8]. Zhao et al. proposed a new method that can be used to predict the springback for profile with any cross section [9]. Zhao et al. bulit the three-dimensional finite-element model for thin-walled tube bending under the ABAQUS/Explicit [10]. Paulsen and Welo concluded that numerical simulation is a well-suited tool for design optimization in the bending of profile [11]. Clausen et al.

designed suitable stretch-bending parameters to reduce springback and cross distortion for car bumpers [12]. Elsharkawy and El-Domiaty determined the stretch bendability limits and springback [13].

In this paper, for the asymmetric L-section aluminum alloy profiles, the numerical simulation technology is used to simulate the flexible stretch-bending process. The influence of the curvature of the MPD surface on stress-strain distribution, shape accuracy, and springback was studied, and the optimal shape of the contact area between the MPD and the profile was determined. Finally, we determine the selection range of curvature of MPD surface for workpiece with a bending radius of 2700 mm.

2. Flexible Multipoint Stretch-Bending Process and Finite Element Model

2.1. Flexible Multipoint Stretch Bending. Flexible 3D multipoint stretch-bending technology is an advanced, rapid manufacturing technology. It has bending deformation in two mutually perpendicular planes in three-dimensional space, and compared with the soild die, the MPD surface can be reconstructed. The solid die is divided into several segments; each segment is called a unit body as a unit of the flexible MPD. The unit is called a flexible fundamental unit (FFU). The FFU can be moved back and forth along the T-shaped groove of the die base to control the horizontally curved die surface, and the MPD body moves in the vertical direction along the lead screw when vertically bent. Figure 1 shows the schematic view of a flexible multipoint stretch bending.

The flexible multipoint bending machine can process profiles from 1.5 m to 7.5 m, and the center spacing of two FFU is 238. 25 mm. The minimum radius of curvature of the forming is 1340 mm in the horizontal direction. The process sequence of the three-dimensional multipoint bending process is MPD location adjustment, prestretching, stretch bending, poststretching, and unloading.

2.2. Material Models. The material used in this paper is aluminum alloy grade AA6082. It is assumed that the profile has an isotropic hardening rule, and von Mises yield criterion is specified. The mechanical properties were measured by the uniaxial tensile test. The relevant performance parameters of AA6082 aluminum alloy are shown in Table 1. The true stress and true plastic strain relationship was obtained through a single tensile experiment as follows:

$$\sigma = \sigma_y + \sum_{i=1}^{2} Q_i\left(1 - e^{-C_i+\xi_p}\right). \tag{1}$$

2.3. Establishment of Finite Element Model. This paper uses ABAQUS 6.14 software for numerical simulation. The ABAQUS/Explicit dynamic explicit algorithm was used to simulate the forming process; the ABAQUS/Standard static implicit algorithm was used to simulate the springback process. Due to the symmetry of profile bending shape and operation, 1/2 model was adopted to reduce the simulation time.

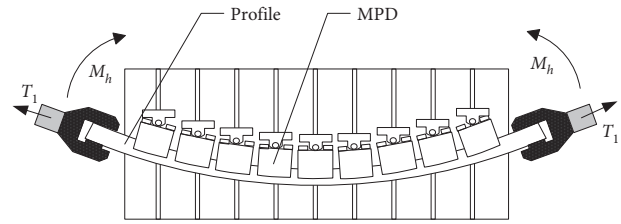

Figure 1: Schematic diagram of flexible multipoint drawing.

Table 1: AA6082 aluminum alloy material parameters.

E (MPa)	ν	σ_y (MPa)	Q_1 (MPa)	C_1	Q_2 (Mpa)	C_2
71000	0.345	139.5	17	2300	168	13

Note. E represents the modulus of elasticity, ν represents Poisson's ratio, σ_y represents the yield stress, and Q_i and C_i are material parameters.

The aluminum profile is modeled using C3D8R, an 8-node linear brick, reduced integration, and hourglass control element. The MPDs and clamps are defined as discrete rigid bodies because their strength is much greater than that of aluminum profiles. And using rigid body units can effectively shorten the numerical simulation time. For the sake of simple calculation, the MPD only draws the contact part with the profile and is modeled into ABAQUS 6.14 by CATIA V5R20 software. Figure 2 shows part drawing and assembly drawing in the finite element analysis. The schematic diagram of the shape displacement and rotation angle of the MPD is shown in Figure 3.

According to the geometric relationship, the calculation formula of the i-th MPD displacement is as follows [13]:

$$y_i^2 = \left[2R \sin\frac{(i-1)\theta}{2(n-1)}\right]^2 - [(i-1)d]^2. \tag{2}$$

The calculation formula of the i-th MPD assembly rotation angle is as follows:

$$\varphi_i = \arctan\left[\frac{y_i}{(i-1)d}\right] - \frac{(i-1)\theta}{2(n-1)}. \tag{3}$$

The penalty function method was used for the face to face interaction, and the Coulomb friction model was used for the friction. The friction coefficient was defined as 0.1 through measurement in experiment. A symmetrical fix boundary condition is applied to the profile. Controlling the boundary conditions between the reference point of clamp could drive the forming process of the profile. Firstly, the horizontal displacement is applied to the clamp for prestretching. Then, the movement of clamp is controlled by the displacement-time curve to drive profile bending. Finally, the bending profile is poststretched along the tangent direction of target shape. In this paper, displacement is used to mark the clamp movement. Obtain forming trajectory by calculating the coordinates of each moment of the clamp reference point. The schematic diagram of the forming trajectory of the clamp during the bending process studied is shown in Figure 4.

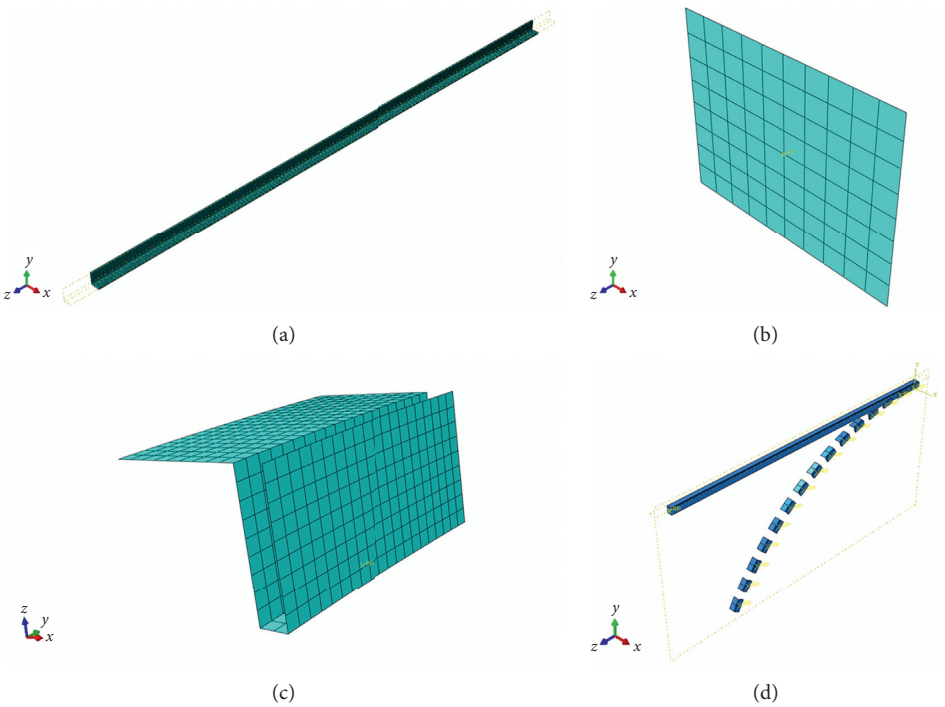

Figure 2: Part drawing and assembly drawing in the finite element analysis: (a) aluminum profile; (b) clamp; (c) MPD; (d) assembly drawing.

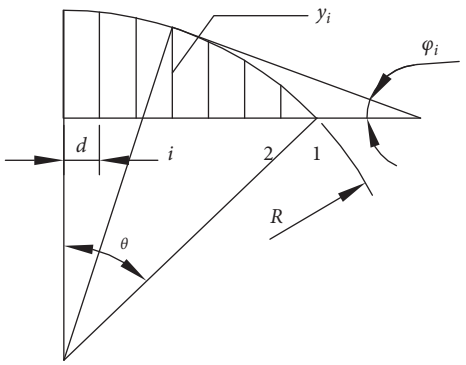

Figure 3: The schematic diagram of the shape displacement and rotation angle of the MPDs.

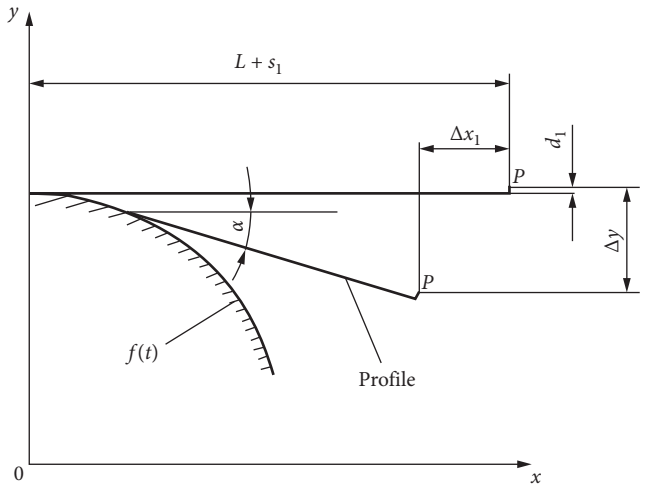

Figure 4: The schematic diagram of the running track of the clamp.

According to the geometric relationship of Figure 4, the displacement calculation formula in the x and y directions can be obtained as follows:

$$\alpha = \arctan f'(t),$$

$$\Delta x_1 = (L = s_1) - \left\{ x(t) = \left[(L = s_1) - \int_0^{x(t)} \sqrt{1 + \tan^2 \alpha}\, dt \right] \cos\alpha + d_1 \sin\alpha \right\}, \quad (4)$$

$$\Delta y = d_1 (1 - \cos\alpha) + y(0) - y(t) + \left[(L + s_1) - \int_0^{x(t)} \sqrt{1 + \tan^2 \alpha}\, dt \right] \sin\alpha,$$

where α is the instantaneous coverage angle when the profile is bent along the x-y plane; t is the projection value of the curved contour of the target on the x-axis; Δx_1 is the displacement of the clamp reference point along the x-y plane toward the x-axis; Δy is the displacement of the clamp reference point along the x-y plane to the y-axis direction; L is one-half length of the profile; s_1 is the pretension of the profile; and d_1 is the distance between the profile lower web and the clamp reference point P.

In the finite element simulation, the forming process and the springback process are divided into two models. ABAQUS/Explicit is used to simulate the forming process.

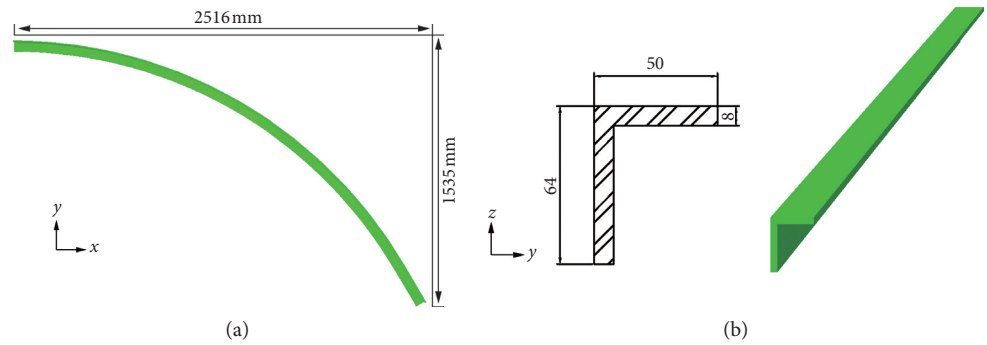

Figure 5: Flexible stretch-bending part. (a) Vertical view of target forming shape. (b) Geometrical parameters of the aluminum profile section.

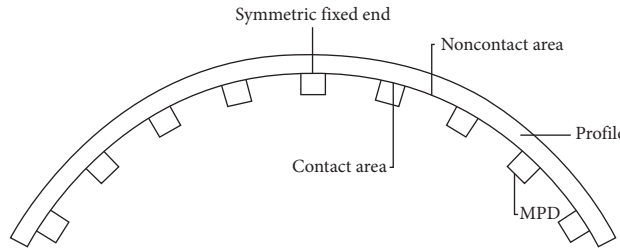

Figure 6: The schematic diagram of the selection of the contact area and the noncontact area.

There are three analysis steps: prestretching, bending, and poststretching. Use ABAQUS data transfer to perform springback simulation using ABAQUS/Standard. Remove all parts except the profile, remove all interaction and boundary conditions, and apply appropriate boundary conditions to the profile to fix the profile side.

3. Numerical Simulation Results and Discussion

In the flexible multipoint bending process, the stress-strain distribution, shape accuracy, and springback of the formed part are affected by the different MPD surfaces. Therefore, the design of the MPD in the multipoint stretch bending process is crucial. Figure 5 shows the geometrical parameters of the aluminum profile. The prestretching amount is 1.5% of the length of the profile, the poststretching amount is 1%, and the number of MPDs is 15.

Different MPD surface curvatures are selected to simulate the flexible stretch-bending process to determine the most suitable MPD geometry. The profile length is 6000 mm, the target bending radius is 2700 mm, and the bending angle is 120°. In this section, MPDs have a radius of curvature of 100 mm, 500 mm, 1000 mm, 2000 mm, 2500 mm, 2600 mm, 2700 mm, 3500 mm, 4500 mm, 5500 mm, and 6500 mm. And the MPDs have a width of 100 mm. A total of 15 MPDs were selected in the numerical simulation, so there are 14 gaps between the MPDs to sequentially number the MPDs from the symmetrical end of the profile to the clamp direction—number 1 to number 14. The schematic diagram of the selection of the contact area and the noncontact area is shown in Figure 6. The contact point of the contact area is the contact point between the profile and the MPD body, and the noncontact area is selected as the midpoint of the profile in the noncontact area. Since the stress concentration occurs in the transition area between the last MPD and the clamp, the transition area is cut off after the forming is completed. Therefore, only the effective forming area is selected for analysis.

3.1. Influence of MPD Curvature on Stress-Strain Distribution. Figure 7 shows stress distribution of the MPD surface radius of curvature of 100 mm, 2000 mm, and 2700 mm. The linear MPD of loaded profile has no transition zone before springback. Figure 8 shows the equivalent plastic strain distribution. Figure 9 shows the maximum stress and the maximum equivalent plastic strain when curvature of MPDs changes after stretch bending.

As the radius of curvature of the MPD is closer to the curvature of target shape, the maximum stress and equivalent plastic strain are smaller. As the radius of curvature of the MPD increases closer to the target curvature, the smaller the maximum stress-strain distribution range, the more uniform the stress-strain distribution. When the radius of curvature of the MPD surface is smaller than the target shape, the contact area between the MPDs and profile is too small, resulting in stress concentration, which affects the forming quality, and especially in some severe cases, it will form defects such as indentation. When the curvature of MPD is close to the target, no defects will occur, and the stress-strain distribution will be more uniform. When the radius of curvature of MPD is larger than the target shape, the stress-strain will increase with the radius of curvature of

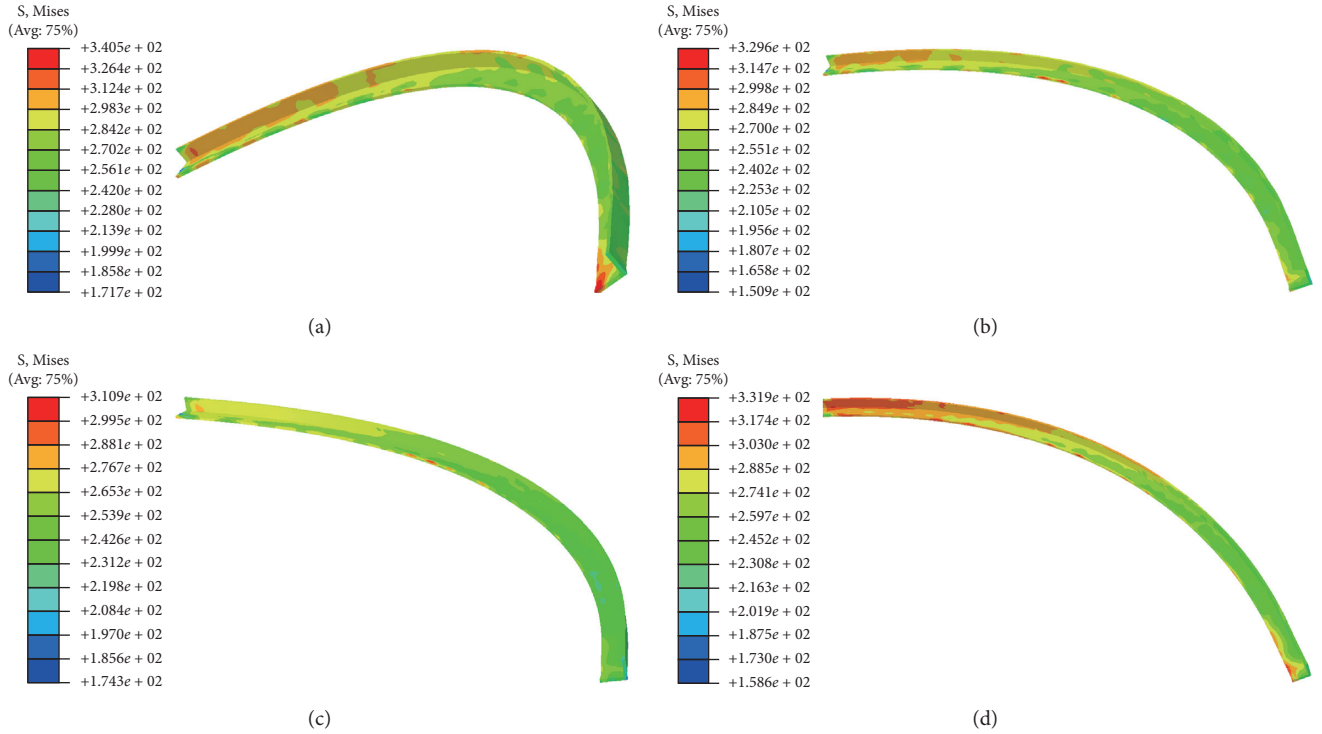

FIGURE 7: The equivalent stress distribution of the profile after the stretch bending: (a) the radius of curvature of MPDs: $r = 100$ mm; (b) the radius of curvature of MPDs: $r = 2000$ mm; (c) the radius of curvature of MPDs: $r = 2700$ mm; (d) straight MPD.

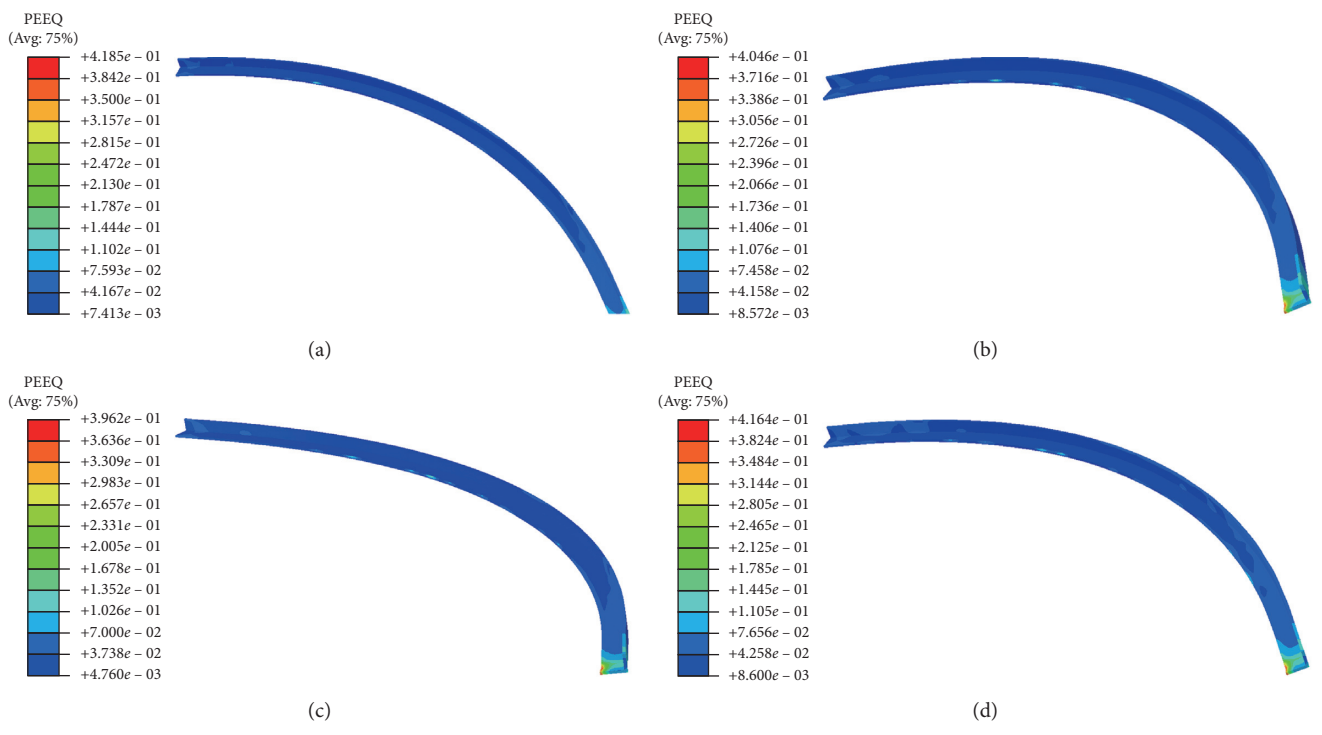

FIGURE 8: The equivalent plastic strain distribution of the profile after the stretch bending: (a) the radius of curvature of MPDs: $r = 100$ mm; (b) the radius of curvature of MPDs: $r = 2000$ mm; (c) the radius of curvature of MPDs: $r = 2700$ mm; (d) straight MPD.

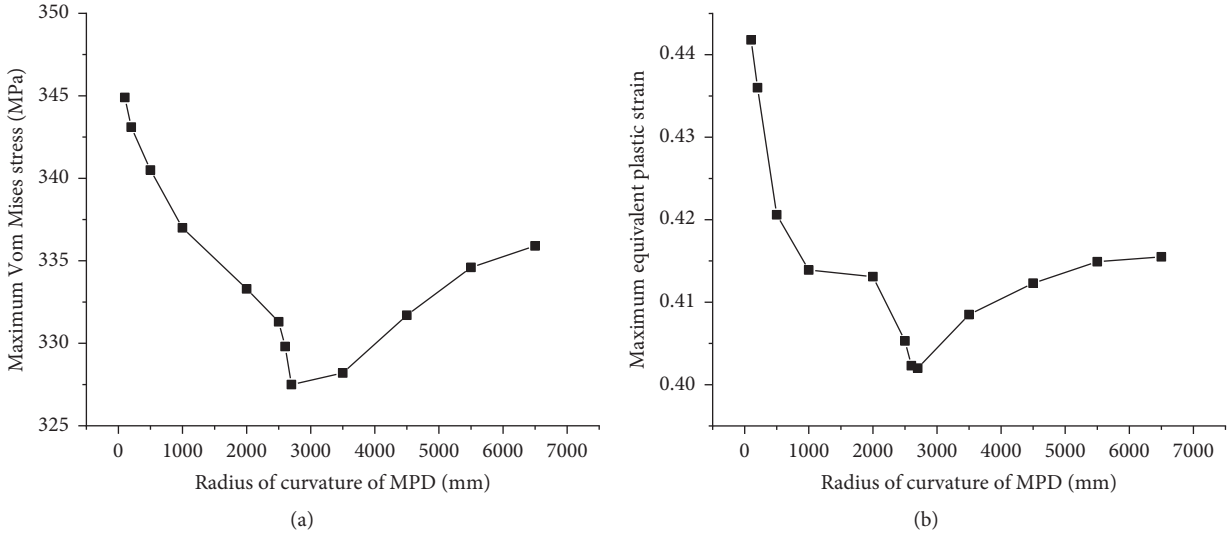

Figure 9: The maximum stress and the maximum equivalent plastic strain when curvature of MPDs change: (a) the relationship between the maximum stress and radius of curvature of MPD; (b) the relationship between the maximum equivalent plastic strain and radius of curvature of MPD.

the MPD. The reason is that the formed envelope surface is composed of a plurality of discrete MPD profile faces, and the larger the radius of curvature of the MPD, the edge of the MPD body will deviate from the target shape, further generating stress concentration again.

Figure 10 shows the distribution of stress-strain in the contact area and noncontact area of the radius of curvature of different MPDs. It can be seen that the stress-strain between the contact area and the noncontact area increases as the position approaches the clamp. The stress in the contact area between the profile and the MPD is significantly greater than the stress in the noncontact area. When $r = 100$ mm, the contact area and the noncontact area have a large difference in stress due to the small contact area with the profile; when MPDs are linear, the edge of the MPD deviates from the target shape, so the part is creased here. And owing to the difference of the contact area, the stress-strain in the noncontact area is also very large. When r=2000 mm and $r = 2700$ mm, the envelope MPD surface and the noncontact area have the least difference in stress-strain, which means the stress-strain distribution is the most uniform.

3.2. Influence of the Curvature of the MPD on the Shape Error of the Profile. The process consists of an entire envelope surface composed of a plurality of MPDs so that a shape error occurs in a region where the profile and the MPD are not in contact, and the shape error is schematically illustrated in Figure 11.

Figure 12 shows the maximum shape error of the bending of the MPDs with different curvatures. It can be seen that the closer the curvature of the MPDs which is to the target curvature ($r = 2700$ mm), the smaller the shape error. When it is smaller than the target radius, the contact area between the MPDs and the profile is small, the profile is not well supported, and the shape error is large; when it is larger than the target radius, the position of the edge of the MPDs will deviate from the target shape, resulting in large shape error which reduces the accuracy of the forming part. As the radius of the MPD surface increases, the shape error increases less. When the MPD profile is smaller than target, the shape error increases fast. The shape error when $r = 2000$ mm is already larger than the shape error when $r = 6500$ mm, and when r is less than 2000 mm, the shape accuracy requirement is not satisfied.

The shape error of the noncontact area formed by MPD with different curvatures is shown in Figure 13. When $r = 100$ mm, the contact area between the MPD and the profile is too small, and the profile cannot be well supported in processing. As a result, the shape error of the noncontact area is very large, which has exceeded the allowable range of the formed part. As the straight MPD edge deviates from the target shape greatly, the shape error in the noncontact area is also large.

3.3. Influence of the Curvature of the MPD on the Springback. After the profile stretch-bending, due to the release of the stress in the profile, the springback error will directly affect the quality of the formed part. In this paper, the displacement difference in the y-axis direction is used as an index, as shown in Figure 14.

Figure 15 shows the effect of the radius of curvature of the different MPDs on the springback of the profile. It can be seen that when the curvature of the MPD is consistent with the target, the springback is minimal. Due to the different curvatures of the MPD, the springback of the MPD after forming is different. Therefore, for the MPD profile, selecting the MPD that conforms to the curvature of the target forming part can effectively reduce the springback error.

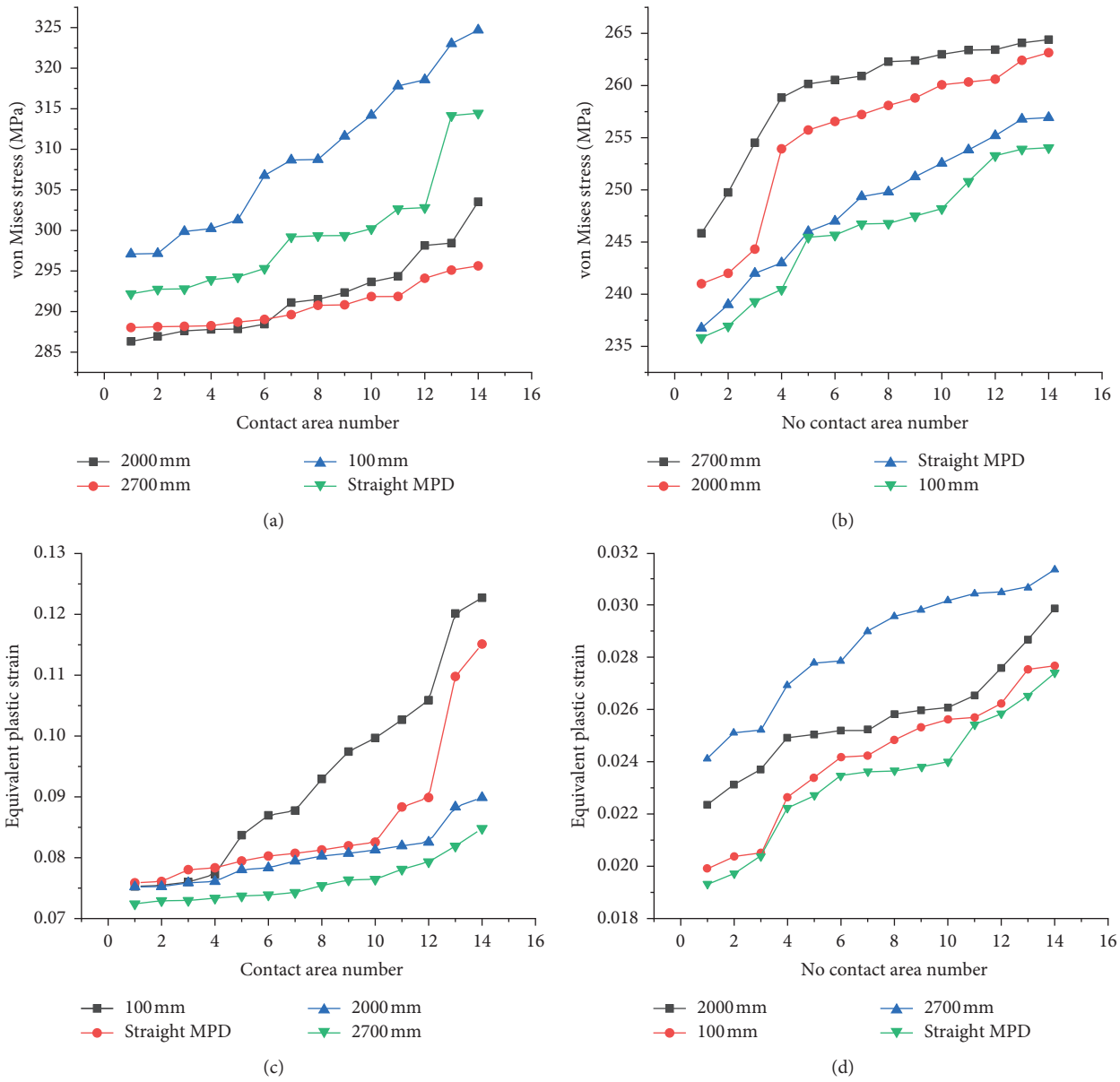

Figure 10: The distribution of stress-strain in the contact area and noncontact area of the radius of curvature of different MPDs: (a) the distribution of stress in the contact area; (b) the distribution of stress in noncontact area; (c) the distribution of strain in the contact area; (d) the distribution of strain in noncontact area.

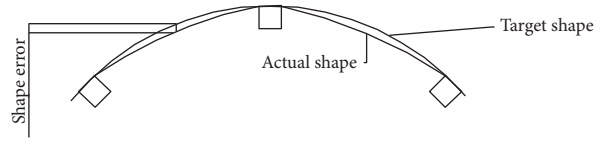

Figure 11: The schematic diagram of the shape error.

4. Experiment

In this paper, the flexible multipoint stretch-bending test was carried out to verify the reliability of the simulation, taking the frame of a high-speed railway car as an example (as shown in Figure 16). The test process is as follows: firstly, the aluminum profile is bent by using the FSB equipment prototype, and then the springback value of the profile is measured by the springback detection tool three times to reduce measurement error. The comparison between experimental results before and after optimization the curvature of MPDs is shown in Figure 17 which also shows the comparison of simulation results and experiment before and after optimization of MPDs. The experimental results are

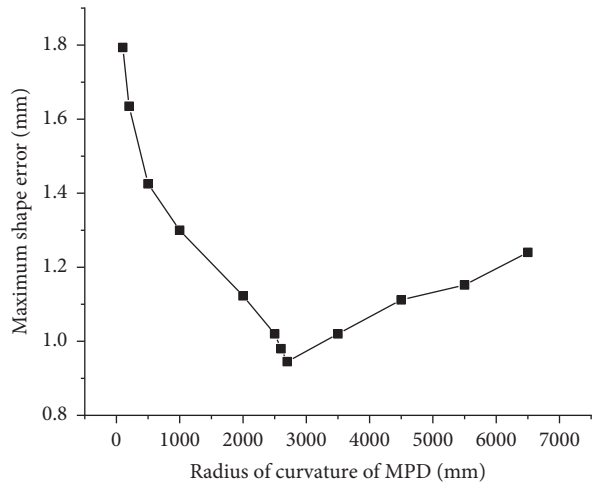

Figure 12: The relationship between the maximum shape error and radius of curvature of MPD.

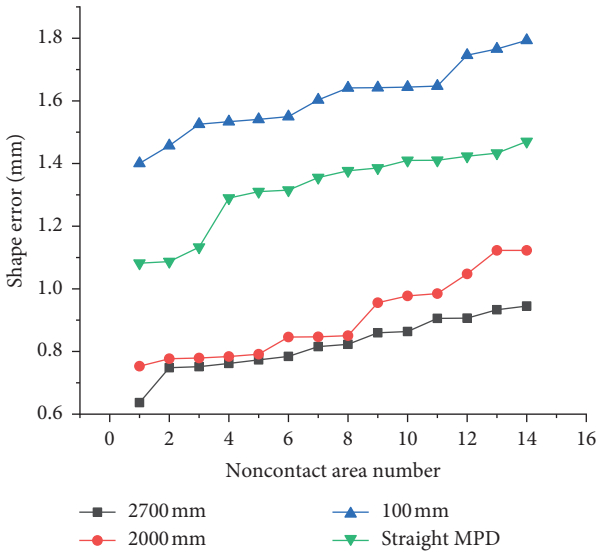

Figure 13: Shape error of the noncontact area formed by MPDs with different curvatures.

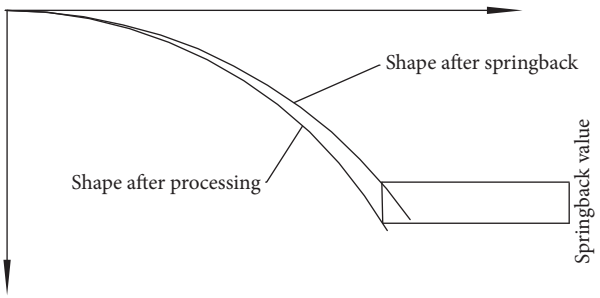

Figure 14: Schematic diagram of springback.

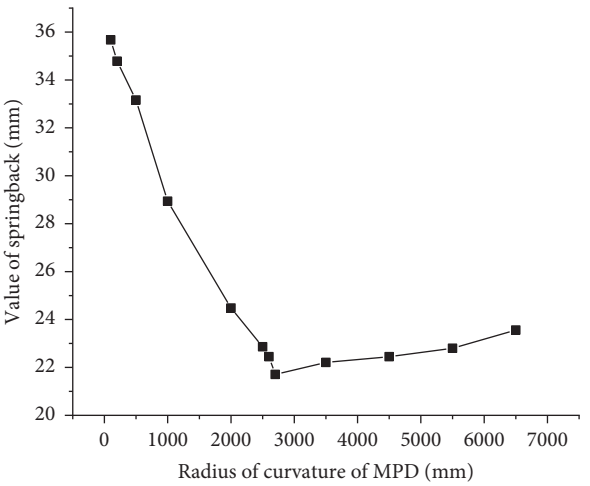

Figure 15: The effect of the radius of curvatures of the different MPDs on the springback of the profile.

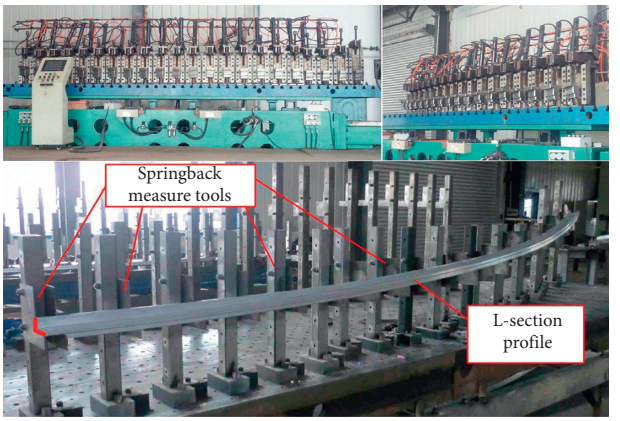

Figure 16: The flexible stretch bending experiment with L-section profile.

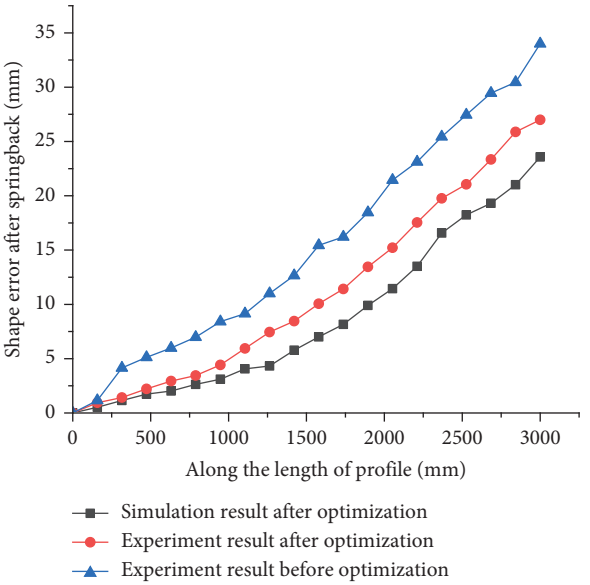

Figure 17: Comparison between the experiment results and the numerical simulation results.

basically consistent with the numerical simulation results. The optimized MPDs can reduce the springback value and improve the shape accuracy.

5. Conclusion

(1) When the curvature of MPD is consistent with the target shaped parts, the shape error and springback value are minimum.

(2) When the curvature of MPD closes to the target part, the stress-strain distribution between the noncontact area and the contact area with the profile will be more uniform.

(3) When the curvature radius of MPD is smaller than that of the target part, the shape error and springback increase greatly as the radius decreases; when the radius is larger than the target shape, the shape error and springback increase less as the radius increases.

(4) For the target shape $r = 2700$ mm, the radius of curvature of MPD is between 2000 mm and 4500 mm, and the error is within the allowable range.

(5) The flexible multipoint stretch-bending test for the profile was carried out. The test results showed that they are in agreement with the simulation results. For this purpose, the forming parameters can be optimized by the finite element simulation to guide the production test and reduce the production cost.

Data Availability

The data used to support the findings of this study are available from the corresponding author upon request.

Conflicts of Interest

The authors declare that there are no conflicts of interest regarding the publication of this paper.

Acknowledgments

This work was financially supported by the National Science Foundation of China (51675225), Project of Jilin Provincial Scientific and Technological Department (20180201074GX, 20190201110JC, and 20190302037GX), Project of Jilin Provincial Development and Reform Commission (2019C046-2), and Project of Education Department of Jilin Province (JJKH20180130KJ).

References

[1] E. Corona, "A simple analysis for bend-stretch forming of aluminum extrusions," *International Journal of Mechanical Sciences*, vol. 46, no. 3, pp. 433–448, 2004.

[2] M. Yoshida, F. Yoshida, H. Konishi, and K. Fukumoto, "Fracture limits of sheet metals under stretch bending," *International Journal of Mechanical Sciences*, vol. 47, no. 12, pp. 1885–1896, 2005.

[3] M. Takamura, M. Sakata, A. Fukui et al., "Investigation of twist in curved hat channel products by elastic-plastic finite element analysis," *International Journal of Material Forming*, vol. 3, no. S1, pp. 131–134, 2010.

[4] S.-l. Zang, M.-G. Lee, L. Sun, and J. H. Kim, "Measurement of the Bauschinger behavior of sheet metals by three-point bending springback test with pre-strained strips," *International Journal of Plasticity*, vol. 59, pp. 84–107, 2014.

[5] Ji C. Liang et al., "Flexible 3D stretch-bending technology for aluminum profile," *The International Journal of Advanced Manufacturing Technology*, vol. 71, no. 9–12, pp. 1939–1947, 2014.

[6] P. H. Vatter and R. Plettke, "Process model for the design of bent 3-dimensional free-form geometries for the three-roll-push-bending process," *Procedia CIRP*, vol. 7, no. 5, pp. 240–245, 2013.

[7] Z.-Y. Cai, S.-H. Wang, X.-D. Xu, and M.-Z. Li, "Numerical simulation for the multi-point stretch forming process of sheet metal," *Journal of Materials Processing Technology*, vol. 209, no. 1, pp. 396–407, 2009.

[8] X. Lin, Y. Li, Z. Cai et al., "Effect of flexible 3D multipoint stretch bending dies on the shape accuracy and the optimal design," *Advances in Materials Science and Engineering*, vol. 2018, pp. 1–9, 2018.

[9] J. Zhao, R. Zhai, Z. Qian, and R. Ma, "A study on springback of profile plane stretch-bending in the loading method of pretension and moment," *International Journal of Mechanical Sciences*, vol. 75, pp. 45–54, 2013.

[10] G. Y. Zhao, Y. L. Liu, H. Yang, C. H. Lu, and R. J. Gu, "Three-dimensional finite-elements modeling and simulation of rotary-draw bending process for thin-walled rectangular tube," *Materials Science and Engineering: A*, vol. 499, no. 1-2, pp. 257–261, 2009.

[11] F. Paulsen and T. Welo, "Application of numerical simulation in the bending of aluminium-alloy profiles," *Journal of Materials Processing Technology*, vol. 58, no. 2-3, pp. 274–285, 1996.

[12] A. H. Clausen, O. S. Hopperstad, and M. Langseth, "Stretch bending of aluminium extrusions for car bumpers," *Journal of Materials Processing Technology*, vol. 102, no. 1–3, pp. 241–248, 2000.

[13] A. A. Elsharkawy and A. A. El-Domiaty, "Determination of stretch-bendability limits and springback for T-section beams," *Journal of Materials Processing Technology*, vol. 110, no. 3, pp. 265–276, 2001.